Heliyon 9 (2023) e15539

Contents lists available at ScienceDirect

Heliyon

journal homepage: www.cell.com/heliyon

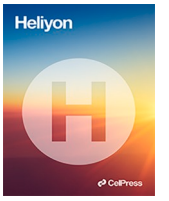

Research article

microRNA-96 targets the INS/AKT/GLUT4 signaling axis: Association with and effect on diabetic retinopathy

Narges Zolfaghari [a], Zahra-Soheila Soheili [a,*], Shahram Samiei [b], Hamid Latifi-Navid [a], Ali Hafezi-Moghadam [c], Hamid Ahmadieh [d], Mozhgan Rezaei-Kanavi [e]

[a] *Department of Molecular Medicine, National Institute of Genetic Engineering and Biotechnology, Tehran, Iran*
[b] *Blood Transfusion Research Center, High Institute for Research and Education in Transfusion Medicine, Tehran, Iran*
[c] *Molecular Biomarkers Nano-Imaging Laboratory, Brigham and Women's Hospital, Boston, MA, USA*
[d] *Ophthalmic Research Center, Research Institute for Ophthalmology and Vision Science, Shahid Beheshti University of Medical Sciences, Tehran, Iran*
[e] *Ocular Tissue Engineering Research Center, Research Institute for Ophthalmology and Vision Science, Shahid Beheshti University of Medical Sciences, Tehran, Iran*

A R T I C L E I N F O

Keywords:
Diabetic retinopathy
Mmu-miR-96-5p
RT-qPCR
INS/AKT/GLUT4 signaling pathway
Recombinant AAV-2
STZ induced Diabetic mice

A B S T R A C T

Background: miR-96-5p is a highly expressed microRNA in the retina of subjects with diabetes. The INS/AKT/GLUT4 signaling axis is the main cell signaling pathway of glucose uptake in cells. Here, we investigated the role of miR-96-5p in this signaling pathway.
Methods: Expression levels of miR-96-5p and its target genes were measured under high glucose conditions, in the retina of streptozotocin-induced diabetic mice, in the retina of AAV-2-eGFP-miR-96 or GFP intravitreal injected mice and in the retina of human donors with diabetic retinopathy (DR). MTT, wound healing, tube formation, Western blot, TUNEL, angiogenesis assays and hematoxylin-eosin staining of the retinal sections were performed.
Results: miR-96-5p expression was increased under high glucose conditions in mouse retinal pigment epithelial (mRPE) cells, in the retina of mice receiving AAV-2 carrying miR-96 and STZ-treated mice. Expression of the miR-96-5p target genes related to the INS/AKT/GLUT4 signaling pathway was reduced following miR-96-5p overexpression. mmu-miR-96-5p expression decreased cell proliferation and thicknesses of retinal layers. Cell migration, tube formation, vascular length, angiogenesis, and TUNEL-positive cells were increased.
Conclusions: In in vitro and in vivo studies and in human retinal tissues, miR-96-5p regulated the expression of the PIK3R1, PRKCE, AKT1, AKT2, and AKT3 genes in the INS/AKT axis and some genes involved in GLUT4 trafficking, such as Pak1, Snap23, RAB2a, and Ehd1. Because disruption of the INS/AKT/GLUT4 signaling axis causes advanced glycation end product accumulation and inflammatory responses, the inhibition of miR-96-5p expression could ameliorate DR.

* Corresponding author. Department of Molecular Medicine, National Institute of Genetic Engineering and Biotechnology (NIGEB), Shahrak-e-Pajoohesh, 15th Km, Tehran -Karaj Highway, Tehran. P.O. Box: 14965/161, Iran.
E-mail addresses: soheili@nigeb.ac.ir, zssoheili@gmail.com (Z.-S. Soheili).

https://doi.org/10.1016/j.heliyon.2023.e15539
Received 25 January 2023; Received in revised form 7 April 2023; Accepted 13 April 2023
Available online 18 April 2023

1. Introduction

Diabetic retinopathy (DR) is the primary cause of visual impairment in the working age population worldwide. DR is induced by metabolic abnormalities in the retina of subjects with diabetes mellitus (DM). It is a manifestation of endothelial dysfunction characterized by breakdown of the blood–retinal barrier (BRB) and neovascularization [1,2]. Prolonged exposure to hyperglycemia is directly associated with DR development, and the pathological stages of DR follow the progression of retinal blood vessel damage [3,4]. However, because multifactorial etiologies underlie the process of DR development, there is currently no effective available cure for DR [5].

Retinal pigment epithelial (RPE) cells are most vulnerable to damage by hyperglycemia through several signaling pathways, including reactive oxygen species (ROS) production, impairment of metabolic pathways such as oxidative stress, production of proinflammatory mediators, and vascular endothelial growth factor (VEGF) secretion during relevant metabolic processes [6–8]. Degeneration or dysfunction of RPE cells contributes to DR progression. Accordingly, further investigations on the dysfunction of RPE cells under high glucose (HG) culture conditions can mimic DR in vitro and could be considered an essential approach for developing effective therapeutic strategies against DR [9].

The INS/AKT/GLUT4 signaling pathway influences whole-body glucose homeostasis. The binding of insulin to its receptor triggers cascades in the cells, including the IRS1/AKT axis. AKT activation allows GLUT4 translocation onto the cell surface, a process involving several proteins. GLUT4 promotes glucose uptake, reduces blood sugar levels, and allows the recipient cells to absorb the main type of sugar in blood [10]. High levels of glucose in blood lead to the formation of advanced glycation end products (AGEs), which initiate inflammatory signaling pathways [11]. Table 1 presented some genes and their function related to INS/AKT/GLUT4 signaling pathway.

microRNAs (miRNAs) are well-known molecules that regulate the post-transcriptional expression of their target genes [7,12]. miRNAs are involved in the development of various diseases such as cancer, diabetes, and diabetic complications [7,13]. Recent studies have reported that the abnormal expression of several miRNAs is involved in the pathogenesis of DR [7,14–16]. Therefore, miRNAs could serve as potential novel therapeutic agents that can manipulate pathological pathways in DR [17]. The polycistronic miR-183 cluster includes three homologous miRNAs (miR-183, miR-96-5p, and miR-182) and plays an important role in the development and normal functions of sensory organs [18]. Fluctuation in the expression level of the cluster members has been observed in pathological conditions, including DR [19–21]. Previous studies have demonstrated that miR-96-5p expression is increased in the retina of the rat model of induced DR. Also, miR-96-5p is significantly downregulated in oxygen-induced retinopathy (OIR) which causes endothelial dysfunction associated with vascular regeneration, and miR-96 overexpression promotes vascular repair by activation of angiogenesis in retinal endothelial cells and by increasing production of VEGF and ANG-2 [22]. However, few investigations have been conducted to understand whether miR-96-5p guides the pathological changes in DR, and role of miR-96 in the progression of DR pathogenesis is still unclear By using systems biology approaches and protein–protein interaction (PPI) network analysis, we investigated how miR-96-5p target genes involved in the DR signaling pathways are interconnected [23].

2. Materials and methods

2.1. Target prediction and pathway analysis of miR-96-5p

The present study used bioinformatics approaches in the following three steps. A: Identifying proteins involved in DR and genes targeted by mmu-miR-96-5p and determining the common proteins between the two gene lists. In this step, proteins associated with

Table 1
Function of some genes in INS/AKT/GLUT4 axis signaling pathway.

Gene	Function	Reference
IRS	A critical molecule in the insulin signaling pathway and the main mediator of insulin-dependent regulation of glucose metabolism in cells. It is also involved in controlling the function of GLUT4, which is responsible for glucose uptake.	[74]
INSR	Activated the insulin signaling pathway. INSR leads to tyrosine phosphorylation of IRS proteins, phosphorylates, and activates phosphatidylinositol 3-kinase (PI3K).	[75–77]
PI3K and AKT	PI3K and the AKT pathways are the most important pathways linking the IRS proteins to the metabolic effect of insulin. The activated stimulates the phosphorylation and inhibition of TBC1D4 and activates Rab-GAP (GTPase-activating protein); this induces GLUT4 trafficking.	[58, 75–80]
PDK	PDK phosphorylates and activates AKT and serum/glucocorticoid-regulated kinase 3 (SGK3).	[75–77]
SGK3	SGK3 is an antagonist of FOXO genes.	[76]
FOXO	FOXOs play important roles in cellular functions such as gluconeogenesis, inflammation, and insulin sensitivity. The activation of FOXO during HG exposure is suggested to be associated with several diabetic complications such as DR. Phosphorylation of FOXOs promotes their interaction with the 14-3-3 protein and consequently results in their degradation.	[59,81,82]
Rac1	Downstream of PI3K, insulin activates the Rho family small GTPase Rac1, which regulates actin filaments in the cell cortex. Insulin stimulates Rac1 activation during actin remodeling, glucose uptake, and GLUT4 translocation on the cell surface.	[10,83]
Pak1	Activated Rac1 also stimulates the serine/threonine kinase Pak1. Inhibition of Rac1 and Pak1 occurs under insulin resistance conditions	[10,83]
Syntaxin-4 and SNAP-23	GLUT4 vesicles arrive and adhere to the cell surface and merge with the plasma membrane (PM). Syntaxin-4 and SNAP-23 on the PM are t-SNAREs involved in GLUT4 exocytosis and are sufficient for vesicle tethering, while VAMP2 on the targeting vesicle is a vSNARE that promotes fusion.	[10,84]

DR were identified through DisGeNET [24,25], STRING [26,27], and PHAROS [28]. The results were merged to create an updated gene list. Additionally, genes targeted by mmu-miR-96-5p were identified through the TargetScan database (http://www.targetscan.org/) [29], and signaling pathways associated with DR were located in the KEGG database [30]. There are potential miR-96-5p binding sites in the 3'-UTR of several mRNAs involved in the INS/AKT/GLUT4 signaling pathway. Finally, the common proteins between DR disease and the genes targeted by mmu-miR-96-5p were determined by analyzing the subscription between the lists. B: Identification of mmu-miR-96-5p target genes upstream and downstream of common proteins and reconstruction of networks. To detect how mmu-miR-96-5p alters the signaling pathways associated with DR, the KEGG database was used to determine miR-96-5p target genes upstream and downstream of the common proteins. Subsequently, the final gene list was created (Table 2). The network was reconstructed on *Homo sapiens* using the GeneMANIA (3.5.1) [31] plugin implemented in Cytoscape (3.7.2) [32]. C: Using network analysis to select specific genes for real-time PCR. Through network analysis, highly interconnected regions (clusters) were determined through the MCODE plugin (http://baderlab.org/Software/MCODE) [33]. The most important nodes were identified based on different kinds of centralities (Degree, Betweenness, Radiality, Closeness, Stress, Centroid Value, Eccentricity, EigenVector, Bridging, Clustering Coefficient, Neighborhood Connectivity, and Topological Coefficient) in a network through CentiScaPe [34,35] and Network Analyzer [36] plugins, and functional enrichment analysis was conducted to learn more about their biological significance with DAVID (Database for Annotation, Visualization and Integrated Discovery) [37] and g:profiler [38] web servers. Three lists of GO terms and their p values were generated independently based on molecular function (GOTERM_MF_FAT), biological process (GOTERM_BP_FAT), and cellular component (GOTERM_CC_FAT). KEGG and Reactome [39] pathway enrichment analyses were also conducted. REVIGO (http://revigo.irb.hr/) [40] and the produced treemap R script were used to summarize and visualize GO terms with the following parameters: “Small (0.5)” for the allowed similarity and “SimRel” for the semantic similarity measure. Fig. 1 A-C shows a schematic illustration of the steps taken during the study. The results of centrality analysis were integrated and categorized to determine each node’s position in the above-mentioned 12 centralities, and important genes (hubs) were selected for real-time PCR analysis.

2.2. DNA construct

The precursor sequence was retrieved from the NCBI database (Gene ID: 723886). Restriction sites of *Kpn*I and *Xho*I enzymes were placed upstream and downstream of the gene, respectively. The gene was synthesized by Biomatik Company (Ontario, Canada),

Table 2
Gene list.

Gene List- *Mus musculus* (mouse)			
common proteins between DR disease and genes targeted by mmu-miR-96-5p		upstream and downstream of common proteins	
Name	Pathway		
AKT1	mmu04370 - VEGF signaling pathway	Pias1	inhibitor of stat1 and NF-KB/RAS signaling
AKT3 PIK3CA		KRAS	RAS signaling- Apoptosis
		Rassf1	RAS signaling- Apoptosis
		Itga3(ITGA)	pi3k/AKT
		Itga11(ITGA)	pi3k/AKT
		Magi1	pi3k/AKT
		Rps6ka6 (RSK)	mTOR signaling/RAS signaling
		MTOR	mTOR signaling
		HIF1-alfa	VEGF signaling pathway
		stat1	VEGF signaling pathway
		NF-KB	VEGF signaling pathway
		AKT2	VEGF signaling pathway
GRB2	mmu04910 - Insulin signaling pathway	Cav1	GluT4 trafficking
IRS1		Ehd1	GluT4 trafficking
Rac1 AKT1		Rac1	GluT4 trafficking
AKT3 PIK3CA		Pak1	GluT4 trafficking
IGF1R		Snap23	GluT4 trafficking
PRKCZ		RAB10	GluT4 trafficking
		RAB2a	GluT4 trafficking
		Flot1 (flotillin1)	insulin signaling/GLUT4 trafficking
		Prkag3 (AMPK)	insulin signaling/GLUT4 trafficking
		Prkar1a (PKA)	insulin signaling
		Eif4e2 (eIF4E)	insulin signaling/Hif1a
		Map2k1 (MEK1)	insulin signaling/mTOR/FOXO
		PIK3R1 (pi3k)	insulin signaling/Hif1a/VEGF
		PIK3CA(pi3k)	insulin signaling/Hif1a/VEGF
FOXO1	mmu04068 - FOXO signaling pathway	FOXO3	FOXO signaling
IGF1R		FOXO4	FOXO signaling
SOD2		SGK3	FOXO signaling
CAT		PDK2	FOXO signaling
PRKCZ	mmu04933 - AGE-RAGE signaling pathway in diabetic complications	PRKCE(PKC)	AGE/RAGE
		Mapk9 (JNK)	AGE/RAGE

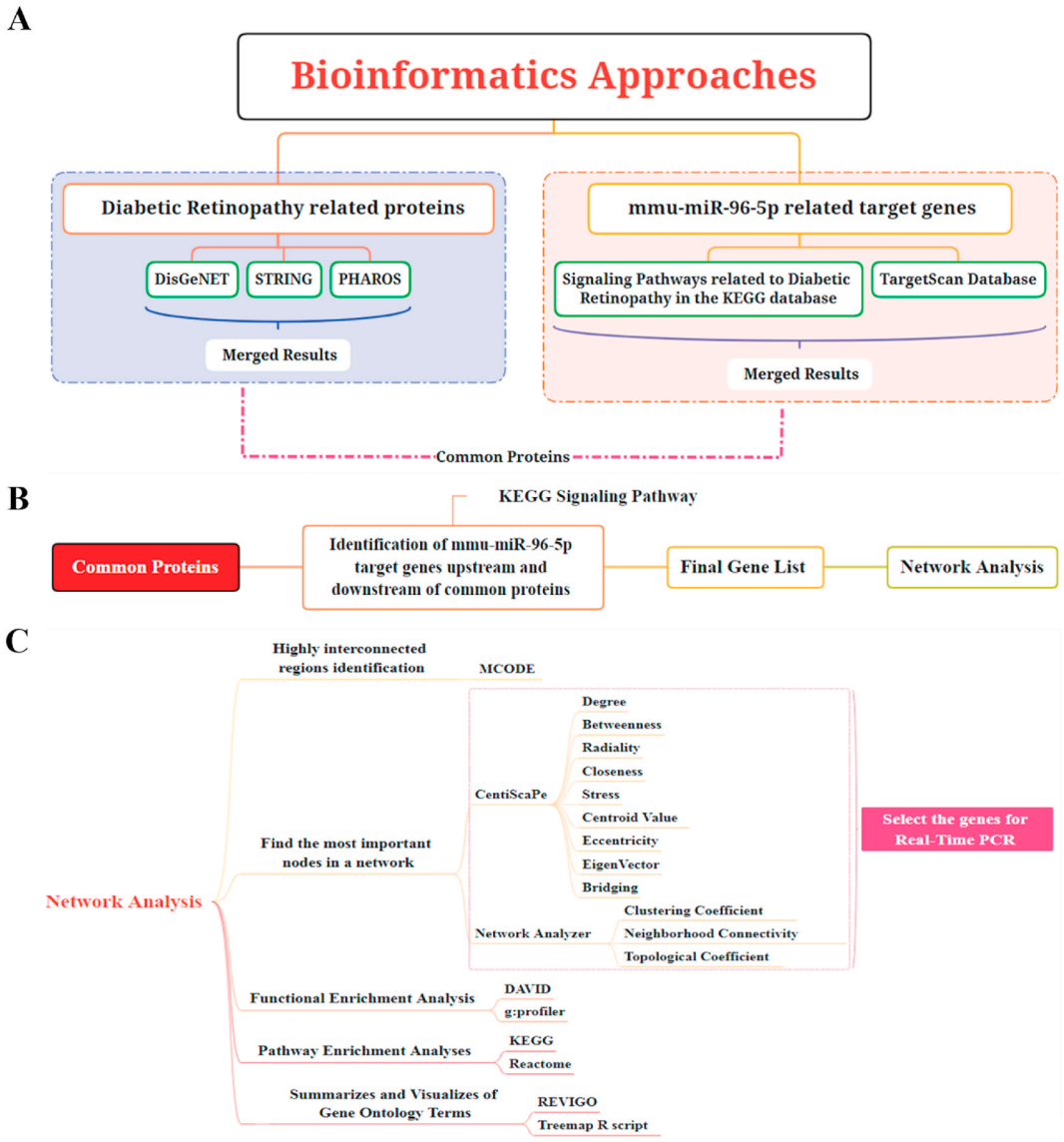

Fig. 1. Diagram illustrating the steps that were taken during the project. **A.** Determine the common proteins between the mmu-miR-96-5p target genes and the proteins involved in diabetic retinopathy. **B.** Analysis of mmu-miR-96-5p target genes upstream and downstream of common proteins and reconstruction of networks. C: Selecting specific genes for Real-time PCR through network analysis.

received in the BSK vector, and subcloned in the pAAV-2-MSC-eGFP vector (a human AAV-2 vector included in the AAV Helper Free System designed by Agilent Technologies, USA, which had been previously constructed in our laboratory adapted from Ref. [41]). Sequence of this vector provided in Supplementary Table S1. Ligation and transformation in *Escherichia coli* XL-10 were performed as described previously [42].

2.3. Cell culture and transfection

mRPE cells were cultured [43] and transfected using the calcium phosphate precipitation method [42,44]. HG culture was established in a 6-well plate with 50% confluency. Cell medium was replaced with serum-free DMEM-F12 1 h before starting the experiment. It was then substituted with DMEM-F12 containing 10% fetal bovine serum (FBS), and the cultures were then treated with 5 mM glucose (as normal glucose concentration) or 30 mM glucose (as HG concentration; Sigma-Aldrich, Germany). Mannitol (Sigma-Aldrich, Germany) at 5 or 30 mM concentration was also applied in parallel cultures as osmotic controls for HG cultures. The cells were incubated in a CO_2 humidified incubator for 48 h. Medium with desired glucose and mannitol concentrations was changed every 24 h.

2.4. mRPE cell treatment with antagomiR-96 and scrambled molecule

To confirm the role of miR-96-5p, its expression was suppressed by antagomiR-96. A scrambled control was also used in independent experiments. A total of 10^6 mRPE cells were plated in a 6-well plate and incubated for 16 h to reach 70% confluency. The cells were transfected with the pAAV-2-MSC-eGFP-mmu-miR-96 vector using the calcium phosphate precipitation method. After 24 h, the cells were transfected again with 30 nM of antagomiR-96 (miRCURY LNA miRNA-96 Inhibitor, YI04102572-DDA, Exiqon) or 30 nM of scrambled control (miRCURY LNA miRNA Inhibitor negative control A, YI00199006-DDA, Exiqon) using Lipofectamine 2000 (Invitrogen, USA) according to the manufacturer's instructions [45]. Finally, at 48 h post-transfection, the cells were collected for further experiments. In another experiment, mRPE cells were cultured under HG conditions as mentioned above. After 24 h, the desired cultures were transfected with antagomiR-96 or scrambled control.

2.5. Cell proliferation assay

mRPE cells were transfected with the pAAV-2-MSC-eGFP-mmu-miR-96 or pAAV-2-MSC-eGFP vector. At 24, 48, and 72 h post transfection, the cells were trypsinized and subjected to 3-(4,5-dimethylthiazol-2-yl)-2,5-diphenyltetrazolium bromide (MTT) assay according to a previously reported protocol [46]. The results were acquired from at least three independent experiments with at least three technical replicates per experiment.

2.6. Wound healing assay

Scratch wound assay was performed to investigate the effect of miR-96-5p on mRPE cell migration. Briefly, cells were transfected with the pAAV-2-MSC-eGFP-mmu-miR-96 or pAAV-2-MSC-eGFP vector as control or with the pAAV-2-MSC-eGFP-mmu-miR-96/antagomiR-96 or pAAV-2-MSC-eGFP-mmu-miR-96/scrambled vector 48 h before starting the assay. Untreated cultures were used as controls. When the cultures reached full confluence, a wound was made using a 100 μL pipette tip. The cells were washed to remove cellular debris. Twenty-four hours later, images were acquired from the cultures and analyzed by the plugin wound_healing_size_tool from Fiji (Fiji Is Just ImageJ-National Institute of Health, Bethesda, MD). The photos were obtained from three independent experiments in at least 3 technical repeats each time.

2.7. Tube formation assay

mRPE cells were transfected with the pAAV-2-MSC-eGFP or pAAV-2-MSC-eGFP-mmu-miR-96 vector in FBS-free DMEM-F12 medium. After 48 h, CM was collected and stored at −80 °C. The 96-well plates were coated with growth factor-reduced matrigel (BD Biosciences, Belgium). HUVECs (3.3×10^4 cells/well) were suspended in 50 μL of the collected CM and were seeded onto the matrigel-coated wells [47]. After 18 h of incubation, the cells were fixed, and images were acquired using an inverted phase contrast microscope (Olympus, Japan). Tube formation ability of the groups was quantified with Fiji software by using an angiogenesis analyzer plugin.

2.8. Plasmids and production and titration of recombinant AAV-2 virus

Two independent AAV-2 virus particles (AAV-2-carrying miR-96 and AAV-2-carrying eGFP as the control) were produced according to a previously published protocol [48]. Viral particles were aliquoted in small volumes and stored at −80 °C. Functional titration of viruses was performed by flow cytometry [49]. GFP expression was measured by flow cytometry assay (CyFlow Space, Partec, Germany) along with FlowMax software. The results were obtained through at least three independent experiments followed by technical repeats.

2.9. Western blot

Whole cell lysates of untreated, GFP-overexpressing, miR-96-5p-overexpressing, miR-96-5p/antagomiR-96-treated, and miR-96-5p/scrambled-overexpressing mRPE cells were prepared using ice-cold RIPA buffer containing protease inhibitors. Total protein samples (15 μg) were separated by 10% SDS-PAGE electrophoresis. Polyvinylidene fluoride (PVDF) membranes (Millipore, Billerica, MA) were used to transfer the proteins. The membranes were then blocked with skimmed milk in TBST and incubated overnight with the following primary antibodies at 4 °C with shaking: mouse anti-Akt1 antibody (sc-5298, Santa Cruz Biotechnology, Germany), mouse anti-PDK2 antibody (SC-100534, Santa Cruz Biotechnology, Germany), rabbit anti-FOXO1 antibody (bs-2537R, Thermo Fisher Scientific, Germany), rabbit anti-FOXO3 antibody (10849-1-AP, Thermo Fisher Scientific, Germany), rabbit anti-PIK3R1 antibody (Orb11271, Biorbyt, United Kingdom), and mouse anti-GAPDH antibody (GTX100118, GeneTex, Taiwan). Subsequently, the membranes were incubated with the appropriate secondary antibodies for 2 h at room temperature (RT) with shaking: HRP-conjugated goat anti-rabbit IgG (BA1054-2, Boster, USA) or HRP-conjugated anti-mouse IgG (SC-516102, Santa Cruz Biotechnology, Germany). Finally, immunoreactive bands were visualized using an ECL reagent (GE Healthcare, UK) and quantified using Fiji analysis software (NIH, Bethesda, MD).

2.10. Experimental animals

Experiments were conducted on 6- to 8-week-old male NMRI mice. Mice were obtained from the National Institute of Genetic Engineering and Biotechnology (NIGEB) animal house. Experiments were performed in accordance with the ARVO (Association for Research in Vision and Ophthalmology) statement for the use of animals and protocols in ophthalmic research and ARRIVE guidelines for the use of laboratory animals. The mice were housed under normal conditions of 12-h light/dark cycle and 20–25 °C temperature, with free access to water and food. For the experiments, the animals were divided into four groups: control, STZ-induced diabetes, AAV-2-eGFP-miR-96 treatment through intravitreal injection, and AAV-2-eGFP treatment through intravitreal injection.

2.11. Establishment of the diabetic mice model

Thirty NMRI mice were randomly divided into control and diabetic groups. Type 1 diabetes was induced by intraperitoneal administration of a single dose (170 mg/kg) of STZ (S0130-1G; Sigma-Aldrich, Germany) prepared in citrate buffer (50 mM Na citrate, pH 4.5 [Sigma-Aldrich, Germany]) immediately before injection. Control mice were injected with an equal volume of Na citrate buffer [50,51]. Diabetes was confirmed to be induced 1 week later on the basis of fasting blood glucose level of >250 mg/dL. STZ-injected animals with fasting blood glucose levels below 250 mg/dL were excluded from the study. The blood glucose level (measured by the Accu-Chek Active kit, Roche, Germany) and weight of the animals were measured once a week. After 10 weeks, mice were sacrificed for further analysis.

2.12. Intravitreal injection

Thirty male NMRI mice were divided into two groups. The right eyes were intravitreally injected with 2 μL of AAV-2 virus particles carrying miR-96 or GFP. Phosphate-buffered saline (PBS) was injected in the left eyes as control eyes. The injections were administered using a Hamilton 5 μL microinjector (CAL7634-01) with an 80 μm glass needle under intraperitoneal anesthesia with a mixture of 100 mg/kg ketamine and 16 mg/kg xylazine. Further analysis was performed two weeks after injection.

2.13. Whole-mount retina, immunohistochemistry, and isolectin B4 staining

To confirm that AAV-2 viral particles were successfully delivered into the retinal cells of the experimental animals, mice were sacrificed by cervical dislocation. The eyes were enucleated and washed with PBS and prefixed in 4% paraformaldehyde for 10 min. The iris and lens were removed, and the retina was carefully separated from the sclera and fixed in ice-cold methanol for 20 min. After washing, tissues were blocked with 1% bovine serum albumin (BSA) at RT for 90 min. The tissues were then incubated with mouse anti-GFP antibodies (sc-9996, 1:100, Santa Cruz Biotechnology, Germany) overnight at 4 °C. On the next day, the tissues were washed with PBS and incubated with FITC-conjugated goat anti-mouse IgG (sc-2010, 1:200, Santa Cruz Biotechnology, Germany) for 2 h at RT. Finally, the tissues were visualized by an Axiophot Zeiss fluorescence microscope. Isolectin B4 staining was performed to reveal the vessels. Whole-mounted retinas were incubated overnight at 4 °C with isolectin B4 (lectin from *Bandeiraea simplicifolia* (L2895, Sigma-Aldrich, Germany), 1:200). Images were acquired using a Leica TCS SPE confocal microscope. AngioTool software was used to quantify the total vessel length and vessels area. The vessels of each retina were observed in three different fields for each studied animal, and the mean value was calculated and compared between all groups.

2.14. HE and terminal deoxynucleotidyl transferase dUTP nick-end labeling (TUNEL) staining

For histological evaluation, the mice were euthanized by cervical dislocation. After washing with PBS, enucleated eyecups were fixed in 4% paraformaldehyde for 16–18 h and then embedded in paraffin. The fixed tissues were cut into 5-μm-thick sections and mounted on microscope slides. HE staining was performed to calculate the thickness of the retinal layers (INL, IRL, and whole retina) according to the standard protocols [52]. Images of each animal's retina were acquired using three different fields and analyzed by Fiji software. TUNEL assay was performed according to the manufacturer's instructions (cat#: 11684817910, Roche, Germany) to detect cell death in the retina. DAPI was used as a nuclear counterstain. Tissues were visualized by an Axiophot Zeiss fluorescence microscope. Three random fields in each section were studied using the retina analysis toolkit, a plugin for Fiji software.

2.15. RNA isolation and quantitative real-time PCR

Total RNA was isolated from treated/control mRPE cells (untreated, GFP-overexpressing, miR-96-5p-overexpressing, miR-96-5p/antagomiR-96-treated, and miR-96-5p/scrambled-treated cells and from cells treated with 5 and 30 mM glucose and 5 and 30 mM mannitol, and cells treated under HG and transfected with antagomiR-96 or scrambled molecule) using the TriPure Isolation Reagent (Roche, Germany) according to the manufacturer's protocol. Total RNA from the retinal tissue of AAV-2-eGFP-miR-96-injected mice, AAV-2-eGFP-injected mice, STZ-induced diabetic mice, and controls were also collected. Retinal tissues of four human DR samples and four healthy controls were obtained from the Central Eye Bank of Iran. All procedures performed in studies involving usage of human retinas for research purpose was approved by the Institutional Review Board of the Central Eye Bank of Iran and were in accordance with the ethical standards of the Helsinki declaration. The Supplementary Table S2 provides the information of donors. The expression level of the genes of interest was quantified using specific primers for real-time PCR analysis (PrimerBank, Harvard) (Supplementary

Table S3). Reverse transcription and amplification were performed using the Qiagen One-Step RT-PCR kit (Qiagen Inc.) and the LightCycler system (Roche, Germany). Hot-start DNA polymerase was activated at 95 °C for 5 min, followed by 35 cycles of 95 °C for 30 s, 60–62 °C for 30 s (depending on the annealing temperature of the genes of interest), and 72 °C for 30 s. According to in silico studies, the results with threshold cycle (Cts) over 35 and melting temperatures below 80 °C were excluded. The stem-loop RT-qPCR procedure was performed as described previously to detect mature miRNAs [53]. First-strand cDNA of miR-96-5p was synthesized using specific stem-loop primers and MMLV enzyme (Qiagen, Germany) as follows: 30 min at 16 °C, 30 min at 40 °C, 5 min at 85 °C, and final holding at 4 °C [42]. Real-time PCR was performed by SYBR Green Master mix (Qiagen, Germany) with a specific forward primer for miRNA-96 and a universal primer using Ampligold Taq polymerase (Roche, Germany). The expression level of mmu-miR-96-5p and the genes of interest were normalized to RNU48 and GAPDH as endogenous controls, respectively. Each sample was assessed in duplicate at least.

2.16. Statistical analysis

Differences between the experimental and control groups were analyzed by one-way analysis of variance (ANOVA) or Student's t-test. The recombinant constructs were transfected into the cells more than three times ($n > 3$) on different days. RT-qPCR and Western blot assays were performed using two independent duplicated samples. In vivo results are expressed as mean ± standard deviation of three biological and technical repeats. Differences with P values < 0.05 were considered statistically significant, and all figures were generated using GraphPad Prism version 8.4.3.

3. Results

3.1. Bioinformatics analysis

3.1.1. A network of genes targeted by mmu-miR-96-5p and DR-related proteins

Subscription results of genes targeted by mmu-miR-96-5p and DR-related proteins were used to reconstruct the PPI network (Supplementary Fig. S1). We used the MCODE plugin of Cytoscape to identify functional complexes (densely connected regions and clusters). Three clusters were identified: 1, 2, and 3 (Supplementary Fig. S2). Cluster scores and the number of nodes in each cluster are shown in Supplementary Table S4. To determine the most relevant KEGG and Reactome pathways associated with each cluster and the entire network, we used the DAVID and g:Profiler databases. The results indicated that cluster 1 nodes were related to Insulin resistance, AGE-RAGE signaling pathway in diabetic complications, and PI3K/AKT signaling in cancer, cluster 2 nodes were associated with the mTOR pathway and signaling by receptor tyrosine kinase and proteoglycans in cancer, and cluster 3 nodes were associated with focal adhesion. Moreover, the nodes of the entire network were associated with the FoxO signaling pathway, insulin signaling pathway, and insulin resistance (Supplementary Table S4).

3.1.2. Enrichment analysis

From the enrichment analysis of the above-mentioned interrelation network, we identified the most relevant concepts underlying GO terms. DAVID databases were used to retrieve GO terms and their P values to construct three networks of molecular functions, cellular components, and biological processes (Supplementary Fig. S3). According to GO terms, the most commonly identified molecular functions were enzyme binding (GO:0019899), kinase activity (GO:0016301), phosphotransferase activity (GO:0016773), and

Table 3
The status of genes in different kinds of centralities.

Gene Name	Bet	Brid	Cent	Close	Deg	Eccent	Eigen	Str	Rad	Clus-Coe	N–C	Topo-Coe
AKT1	+++	–	+++	+++	+++	+++	+++	+++	+++	–	–	–
PIK3R1	+++	–	+++	+++	+++	+++	+++	+++	+++	–	–	–
AKT2	+++	–	+++	+++	+++	+++	+++	+++	+++	–	–	–
PRKCE	+++	++	+++	+++	++	+++	++	+++	+++	–	–	–
PIK3CA	+++	–	+++	+++	+++	+++	+++	+++	+++	++	+	–
AKT3	+++	–	+++	+++	+++	+++	+++	+++	+++	+	+	–
RAB2A	++	++	++	++	++	–	–	+	++	–	–	–
FOXO3	++	++	++	++	++	–	–	++	++	–	–	–
Pak1	++	–	++	++	++	–	+	–	–	–	–	–
PRKCZ	+	–	++	++	+++	–	++	++	++	+++	++	++
FOXO4	–	+++	+	+	+	–	–	+	++	–	–	–
FOXO1	–	–	++	++	++	–	+	+	++	++	+++	++
SNAP23	–	+++	++	++	+	–	–	+	+	–	++	–
IRS1	–	–	++	++	+++	+++	++	++	++	+++	+++	++
EHD1	–	++	+	+	–	–	–	–	–	–	–	–
PDK2	–	+	–	+	–	–	–	–	++	+	–	–
SGK3	–	–	–	–	–	–	–	–	–	+++	+++	+++

(Degree = Deg, Neighborhood Connectivity = N–C, Betweenness = Bet, Bridging = Brid, Centroid = Cent, Clustering Coefficient = Clus-Coe, Closeness = Close, Topological Coefficient = Topo-Coe, Eccentricity = Eccent, Eigenvector = Eigen, <10 = +++, (10–20) = ++, and (21–25) = +. In eccentricity section, 1 = +++, and 2 = -.

protein kinase binding (GO:0019901); commonly identified cellular components were adherens junction (GO:0005912), anchoring junction (GO:0070161), cell junction (GO:0030054), and focal adhesion (GO:0005925); and commonly identified biological processes were intracellular signal transduction (GO:0035556), response to hormone (GO:0009725), response to peptide (GO:1901652), and cellular response to peptide (GO:1901653) (Supplementary Data S1–S3).

3.1.3. Identification of hubs

To identify key nodes (hubs) in the network through various measures of centrality analysis, we used CentiScaPe plugin. The results of comparison between high-degree nodes with other centralities such as betweenness, closeness, eigenvector centrality, centroid value, and bridging are separately shown by scatter plots (Supplementary Figs. S4–S5). Key genes in each of the centralities were identified by classifying the CentiScaPe results from the highest to the lowest scores. The status of a specified gene was evaluated by assigning 1–61 to genes through their order in different centralities. Nodes positioned in 1–25 were considered important genes in the network (Table 3, Supplementary Data S4–S6). The qPCR test was then used to investigate the expression pattern of distinct genes that played key roles in this network.

3.2. In vitro experiments

3.2.1. Cloning and overexpression of pAAV-2-MCS-eGFP-mmu-miR-96

To overexpress miR-96-5p in vitro, the mmu-miR-96-5p gene with flanking sequences was subcloned into the pAAV-2-MCS-eGFP plasmid to yield the pAAV-2-MCS-eGFP-mmu-miR-95-5p plasmid (Supplementary Fig. S6). The successfully obtained recombinant plasmid was then transfected into the mRPE cell line.

3.2.2. miR-96-5p decreased mRPE cell proliferation

The results of three independent MTT assays revealed no significant difference in cellular proliferation between the treatment groups (5 and 30 mM glucose and 5 and 30 mM mannitol cultures). In contrast, in a time-course study, mRPE cells transfected with AAV-2-MCS-eGFP-mmu-miR-96-5p showed a decreased proliferation rate as compared to mRPE cells treated with the control vector

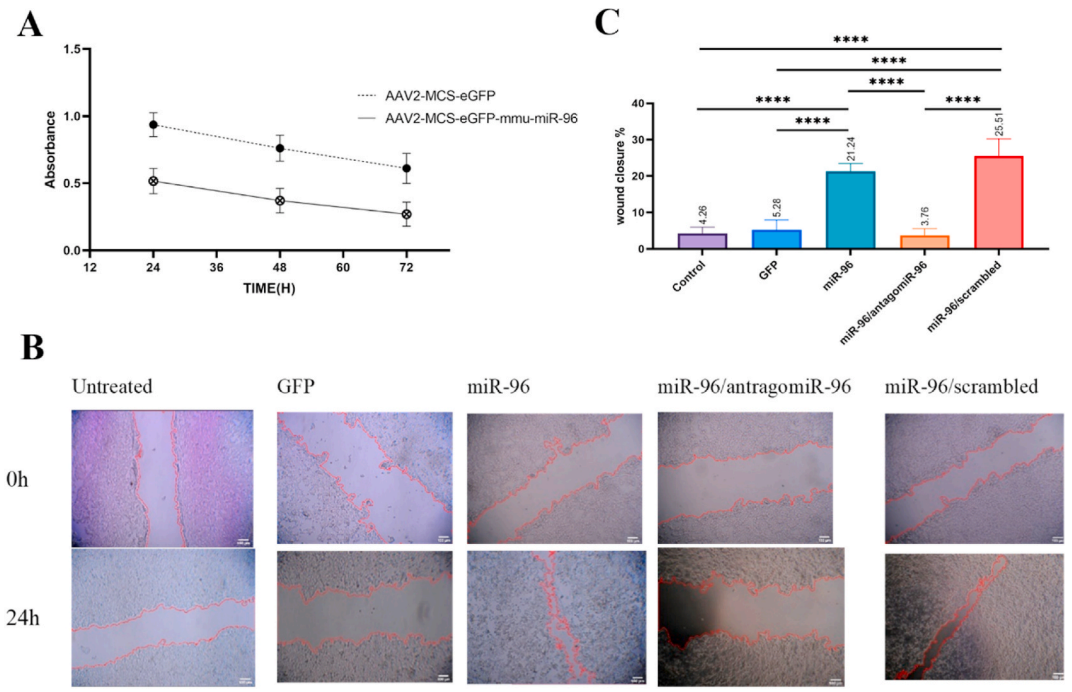

Fig. 2. A. Cell proliferation assay for mRPE cell line transfected by pAAV2-MCS-eGFP-mmu-miR-96 or pAAV2-MCS-eGFP as control. miR-96-5p reduced cell proliferation in comparison to control, 72h after transfection. The plot was drawn using the software GraphPad Prism 8, and *t*-test was used to analyze the data. Results showed significant difference between the treated and control groups ($P < 0.05$) and T test indicated that P value summary symbol is two stars. **B.** miR-96-5p induced cell migration rate in mRPE cells in the scratch assay. The test was performed in five groups, untreated cells, cells treated by control vector (pAAV2-MCS-eGFP), cells transfected by pAAV-MCS-eGFP-mmu-miR-95, miR-96-5p over-expressed mRPE cells simultaneously treated by antagomiR-96 and, miR-96-5p overexpressed mRPE cells simultaneously treated by scrambled molecules. Images were taken in zero times of the tests and after 24h. The scale bar represents 100 μm. **C.** miR-96-5p overexpressed cells and cells treated by scrambled molecules revealed increased migration rate. Data were analyzed using wound_healing_size_tool a plugin for Fiji software. The difference between data represents a statistically significant ($P < 0.0001$) according to the One-way ANOVA. The plot was drawn using the software GraphPad Prism 8.

(AAV-2-MCS-eGFP) (Fig. 2 A).

3.2.3. Migration of mRPE cells increased following miR-96-5p overexpression

Wound healing assay indicated that at 24 h following the expression of mmu-miR-96-5p, the mobility of mRPE cells was increased as compared to that of the control group (mRPE cells transfected with pAAV-2-MCS-eGFP). miR-96-5p-overexpressing mRPE cells simultaneously transfected with antagomiR-96 showed a reduced migration rate as compared to miR-96-5p-overexpressing cultures (Fig. 2 B). miR-96-5p-overexpressing mRPE cells and miR-96-5p/scrambled-overexpressing mRPE cells showed accelerated migration rates toward the scratched area, with a significant average wound closure rate of 21.23% ($P < 0.001$) and 25.5% ($P < 0.001$), respectively, as compared to untreated cells (Fig. 2C). The wound closure rates of untreated cells, GFP-expressing cells, and miR-96-5p/antagomiR-96-overexpressing mRPE cells were not significant after 24 h.

3.2.4. miR-96-5p induced in vitro tube formation in HUVECs

HUVECs treated with conditioned media (CM) of miR-96-5p-overexpressing mRPE cells showed increased tube formation (Fig. 3 A) as compared to the control (CM of GFP-overexpressing mRPE cells). The average number of branching for the HUVEC treated by miR-96-5p overexpressed mRPE CM group and control mRPE cells was 60.70 and 11.2, respectively (Fig. 3C), and the difference was significant ($P < 0.0001$). The former group showed an increased total branching length (mean = 7943.9 vs. 737.6; $P < 0.0001$, Fig. 3 D) and a higher average number of junctions (80.6 vs. 4.4; $P < 0.0001$, Fig. 3 B) than the latter group.

4. Western blot analysis

The expression of AKT1, PDK2, FOXO1, FOXO3, PIK3R1, and GAPDH proteins was detected in whole cell lysates of untreated, GFP-overexpressing, miR-96-5p-overexpressing, miR-96-5p/antagomiR-96-overexpressing, and miR-96-5p/scrambled-overexpressing mRPE cell cultures (Fig. 4 A). Western blot assay revealed that the fold change of FOXO1 and FOXO3 proteins in the cell lysate of untreated, GFP-overexpressing, and miR-96-5p/antagomiR-96-treated cells was decreased by approximately 72% ($P < 0.0001$) and 84% ($P < 0.0001$), respectively (Fig. 4 D and **E)**, as compared to that in the cell lysates of miR-96-5p-overexpressing and miR-96-5p/scrambled-treated mRPE cells. The expression of AKT1, PDK2, and PIK3R1 proteins in untreated, GFP-overexpressing, and miR-96-5p/antagomiR-96-treated cultures was increased by approximately 70% ($P < 0.0001$), 64% ($P < 0.0001$), and 72% ($P < 0.0001$), respectively (Fig. 4 B, C and **F)**. These results suggest that miR-96-5p was involved in the increased expression of FOXO1 and FOXO3 proteins and decreased expression of AKT1, PDK2, and PIK3R1 proteins in mRPE cultures.

4.1. In vivo experiments

4.1.1. Production, titration, and intravitreal injection of recombinant AAV-2 viruses

Viral genomic titer and functional viral titer were estimated as 10^{12} genomic particles/mL and 10^{8} infectious particles/mL, respectively. We injected 2 μL of the particle viruses intravitreally in the mice eye. So that 2 μl intravitreal injection delivered 2×10^{9} genome copies to each eye. Fig. 5 shows anti-GFP antibody-immunostained whole-mount retina from virus or PBS-injected mice (Fig. 5A–C) and negative control (Fig. 5 D).

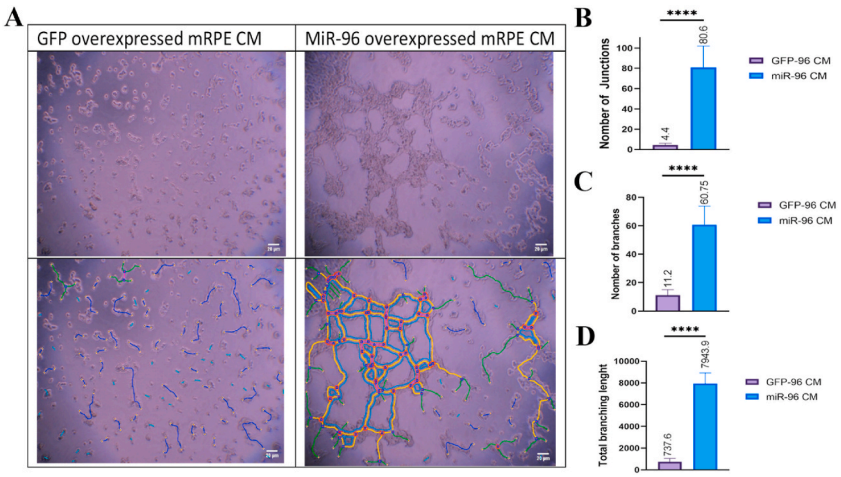

Fig. 3. Matrigel tube formation assay. HUVEC cells were cultured for 16 h in 96-well plates coated with matrigel. **A.** The cells were cultured in miR-96-5p overexpressed mRPE CM or GFP overexpressed mRPE CM (as control). Pictures were analyzed using Angiogenesis Analyzer a plugin for Fiji. The number of junctions (**B**) and branches (**C**) and, total branching lengths (**D**) formed in the assay were measured and analyzed using Student's t-test. *$P < 0.05$ is considered statistically significant. Data were presented as the mean ± standard error of the mean ($N = 6$).

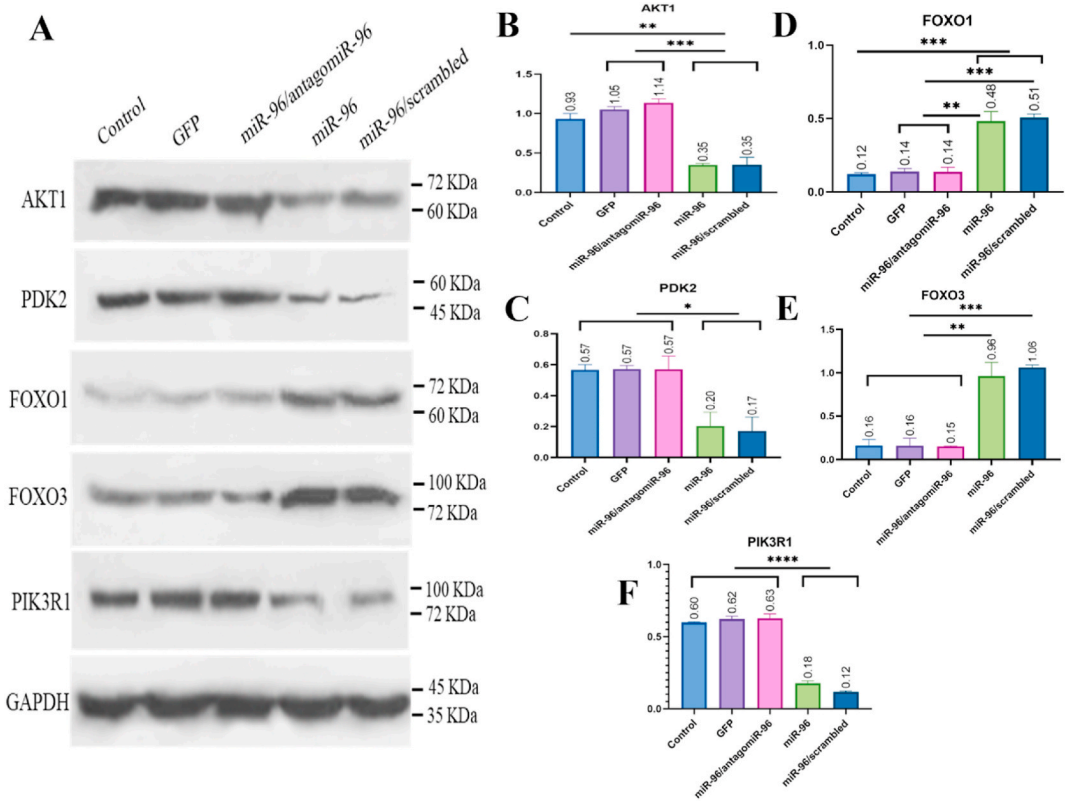

Fig. 4. A. Western blot analysis of AKT1, PDK2, FOXO1, FOXO3, PIK3R1 and, GAPDH for the untreated, GFP overexpressed, miR-96-5p overexpressed, miR-96-5p/antagomiR-96 overexpressed and, miR-96-5p/scrambled overexpressed mRPE cultures' whole-cell lysates. The quantity of proteins for FOXO1(**D**) and FOXO3(**E**) in untreated, GFP overexpressed and, miR-96-5p/antagomiR-96 overexpressed were reduced respected to the miR-96-5p overexpressed and miR-96-5p/scrambled overexpressed groups, while this was completely reversed for AKT1(**B**), PDK2(**C**) and, PIK3R1 (**F**) proteins (full and non-adjusted images are provided in Supplementary Fig. S 8). The protein bands were quantified using Fiji software. The plot was drawn using GraphPad Prism 8. One-way ANOVA test was performed for data analysis. The test was performed in two independent experiments and the calculations were based on three independent determinations. Error bars represent means ± SD (*P < 0.05).

4.1.2. STZ-induced diabetic mice model

Diabetes was induced in mice through an intraperitoneal (i.p.) injection of streptozotocin (STZ). Mice with non-fasting blood glucose levels higher than 400 mg/dL were considered diabetic. Blood glucose level and body weight of the animals were measured every week until 10 weeks after injection (Supplementary Fig. S7). Diabetic mice showed high blood glucose levels and weight loss.

4.1.3. Histological analysis of the retina

Whole-mount retina stained with isolectin B4 from the diabetic, diabetic control, AAV-2-eGFP-miR-96-injected, and AAV-2-eGFP virus-injected mice groups revealed that the total vessel length of the diabetic group was increased as compared to that in the nondiabetic control group. The total vessel length and vessels area were also increased in AAV-2-eGFP-miR-96-injected mice as compared to that in the control (Fig. 6 A-C). Hematoxylin-eosin (HE) staining indicated that INL (inner nuclear layer), IRL (inner retina layer), and whole retina thicknesses in diabetic mice and AAV-2-eGFP-miR-96-treated mice were significantly decreased as compared to that in the control groups (Fig. 6 D-G). TUNEL-positive cells were detected in the GCL (ganglion cell layer), INL, and ONL (outer nuclear layer) layers of AAV-2-eGFP-miR-96-injected mice and in the GCL and INL layers of diabetic mice. No detectable signal was found in the control groups (Fig. 6H and I).

4.2. Gene expression analysis

4.2.1. Gene expression in pAAV-2-MCS-eGFP-mmu-miR-96-treated mRPE cultures

The relative expression of miR-96-5p was increased 13.7-fold in mRPE cells transfected with the pAAV-2-MCS-eGFP-mmu-miR-96 vector as compared to that in GFP-overexpressing cells (Fig. 7 A). Fig. 7 A shows the expression levels of miR-96-5p target genes. The relative expression levels of FOXO1, PDK2, FOXO3, and FOXO4 showed 5.43-, 2.94-, 75.84-, and 1.89-fold increase, respectively, over that of the control cells. In contrast, the expression of several genes in the INS/AKT/GLUT4 signaling pathway decreased as compared to that of the control, e.g., the expression of PIK3R1, PIK3CA, PRKCE, AKT1, AKT2, AKT3, SGK3, Pak1, Snap23, RAB2a, and Ehd1

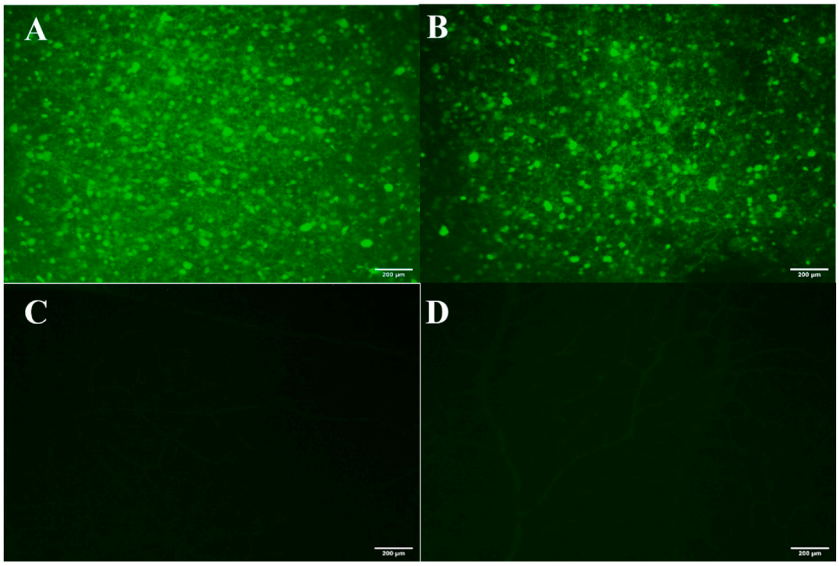

Fig. 5. GFP expression in whole-mount retina from NMRI mice treated by intravitreal injection of recombinant viruses after 2 weeks. **A.** GFP expression in mice retina treated by AAV2-eGFP-miR-96 viruses. **B.** GFP expression in mice retina following injection of AAV2-eGFP viruses intravitreally. **C.** GFP expression in mice retina following PBS intravitreal injection. **D.** negative control, manipulated with just secondary antibody. Images show high infection rate of the recombinant AAV-2 particles (in all experiments N > 8).

decreased by 0.00022-, 0.1-, 0.29-, 0.23-, 0.42-, 0.42-, 0.77-, 0.51-, 0.07-, 0.73-, and 0.025-fold, respectively. The expression of IRS1 remained almost unchanged (1.18-fold) (Fig. 7 A).

4.2.2. Gene expression in miR-96-5p/antagomiR-96- and miR-96-5p/scrambled-overexpressing mRPE cells

The relative expression levels of IRS1, PIK3R1, PIK3CA, PRKCE, Pak1, Snap23, RAB2a, Ehd1, AKT1, AKT2, AKT3, and FOXO3 genes in miR-96-5p/antagomiR-96-overexpressing cells were increased by 13.14-, 2.87-, 1.7-, 3.02-, 3.03-, 5.88-, 10.97-, 3.25-, 3.87-, 3.37-, 2.09-, and 4.47-fold, respectively, as compared to that in miR-96-5p/scrambled-overexpressing cells. Moreover, FOXO1 gene transcripts showed a 0.48-fold decrease in their expression level. The relative expression of FOXO4 remained unchanged (1.07-fold). The expression of PRKCZ and PDK2 was not detected in treated mRPE cells (Fig. 7 B).

4.2.3. Gene expression analysis under HG condition in cultures treated with antagomiR-96 or a scrambled molecule

Total RNA was extracted at 48 h post HG treatment. Gene expression data revealed that miR-96-5p was upregulated (approximately 5-fold) in HG conditions as compared to that in normal glucose-containing media (Fig. 8 A). mRPE cells were cultured under HG conditions, and antagomiR-96 or scrambled molecules were transfected into the cultures. The relative expression levels of genes related to insulin signaling, such as IRS1, following treatment with antagomiR-96 and scrambled molecules were 4.09 and 0.97, respectively. The relative expression levels of PIK3R1, PIK3CA, PRKCE, AKT1, and AKT3 were 0.57 and 0.21, 0.17 and 0.17, 4.21 and 0.89, 0.51 and 0.11, and 0.46 and 0.45, respectively. These findings imply that the above-mentioned genes were downregulated under HG conditions due to miR-96-5p function (Fig. 8). The genes related to GLUT4 trafficking to the cell surface, including Pak1, Snap23, and RAB2a, showed an increased expression level under HG conditions/antagomiR-96 treatment as compared to that under HG conditions/scrambled RNA treatment (Fig. 8 B).

4.2.4. Gene expression in the retina of treated mice

The retina from Naval Medical Research Institute (NMRI) mice with intravitreally injection of AAV-2-eGFP-miR-96 or AAV-2-eGFP viruses were dissected. The retina dissection of STZ-induced diabetic mice group and the control group were also dissected. Total RNAs were isolated, and the expression levels of the desired genes were measured by real-time PCR (Fig. 9 A). The relative expression levels of miR-96-5p, FOXO1, PRKCE, Pak1, Snap23, RAB2a, AKT2, FOXO3, and FOXO4 were increased (5.99-, 5.60-, 9.23-, 6.2-, 4.98-, 9.59-, 1.36-, 1.28-, and 2.33-fold, respectively) in mice injected with AAV-2-eGFP-miR-96 viruses as compared to that in control mice. Moreover, IRS1, PIK3R1, Ehd1, AKT1, AKT3, PDK2, and PRKCZ showed decreased expression (0.76-, 0.93-, 0.61-, 0.88-, 0.79-, 0.75-, and 0.39-fold, respectively) in mice injected with AAV-2-eGFP-miR-96 as compared to that in mice injected with AAV-2-eGFP-carrying viruses. The expression level of PIK3CA (1.05-fold) remained unchanged in the experimental groups.

The expression levels of miR96, IRS1, PIK3R1, PIK3CA, FOXO1, PRKCE, Pak1, Snap23, RAB2a, AKT3, FOXO3, and FOXO4 were increased (52.72-, 2.76-, 2.81-, 1.65-, 9.78-, 3.46-, 8.88-, 2.81-, 2.82-, 1.34-, 16.56-, and 3.31-fold, respectively) in STZ-induced diabetic mice as compared to that in the control group, while the genes Ehd1, AKT2, PDK2, and PRKCZ showed decreased expression (0.34-,0.94-, 0.02-, and 0.12-fold) in diabetic mice as compared to that in the control group. The expression of AKT 1 (1.02-fold) showed no alteration in the studied samples.

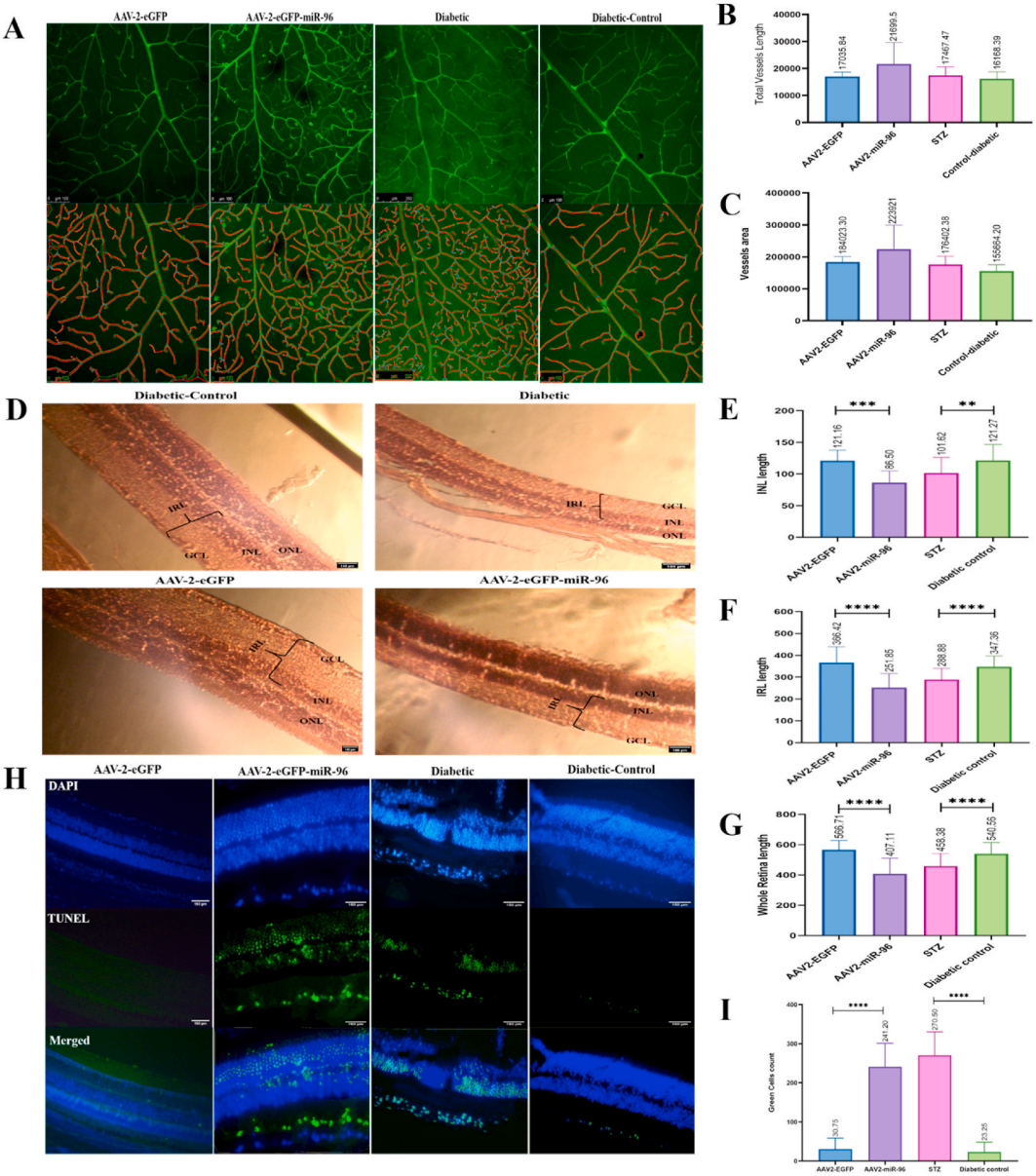

Fig. 6. vascularization, layer thicknesses and cell death analysis in diabetic, non-diabetic, AAV2-eGFP-miR-96 and AAV2-eGFP viruses injected mice. **A.** Isolectin-B4 staining in whole-mount retina of above groups (green channel). Total vessels length (**B**) and Vessels area (**C**) were quantified using AngioTool software. **D.** Hematoxylin-eosin staining in retina of groups described above. INL **(E)**, IRL **(F)** and whole retina thickness **(G)** were measured using Fiji software. **H.** TUNEL assay in retina of above groups, TUNEL (green) and DAPI (blue). **I.** green cells count in TUNEL assay was analyzed using retina-analysis-toolkit, a plugin for Fiji software (mean ± SEM; n = 8; ***P < 0.001). (For interpretation of the references to colour in this figure legend, the reader is referred to the Web version of this article.)

4.2.5. Gene expression in the retina of human donors

The expression of miR-96-5p target genes was measured in the retina of four human donors with diabetes. The relative expression levels of FOXO3 and FOXO4 were increased by 3.7- and 6.75-fold, respectively, over the control retina samples. The expression of several genes related to the INS/AKT/GLUT4 signaling pathway was decreased in diabetic donors as compared to that in the control group, e.g., expression of IRS1, PIK3CA, AKT2, AKT3, PDK2, SGK3, Snap23, RAB2a, and Pak1 decreased by 0.83-, 0.60-, 0.49-, 0.97-, 0.18-, 0.48-, 0.74-, 0.16-, and 0.16-fold, respectively (Fig. 9 B).

5. Discussion

miR-96-5p is a member of the miR-183 family that consists of 3 related miRNAs (miR-183, miR-96, and miR-182); this family is

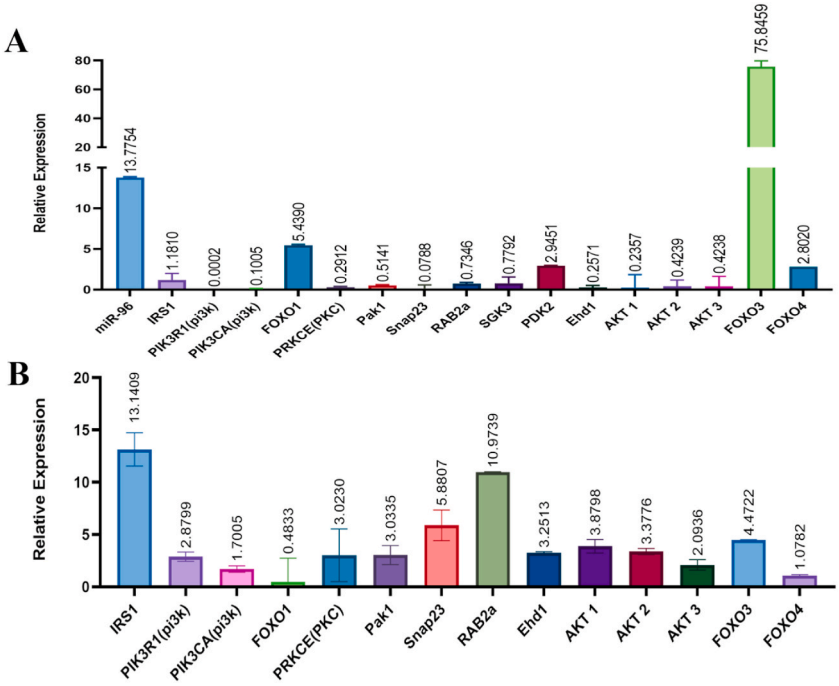

Fig. 7. A. Relative gene expression in mRPE cells transfected by AAV2-MCS-eGFP-mmu-miR-96 in comparison to control mRPE cells transfected with AAV2-MCS-eGFP vector. **B.** Relative expression of miR-96-5p target genes in miR-96-5p overexpressed cells while simultaneously transfected with antagomiR-96 or scrambled molecules. Expression of all the studied genes showed increased relative expression in the presence of miR-96-5p/antagomiR-96 except for FOXO1. The plot was drawn using GraphPad Prism 8 and analyzed with one-way ANOVA test. Each bar describes the mean ± SEM in at least three independent experiments in triplicate. Data differences were statistically significant ($P < 0.001$).

located on the 4-kb conserved region of chromosomes 7q32.2 and 6qA3 in humans and mice, respectively. The expression levels of these miRNAs can be regulated individually by transcription, DNA methylation, and post-transcriptional processing [54,55]. Based on recent findings, the miR-183 cluster is involved in multiple normal physiological processes and pathological conditions such as cell proliferation, apoptosis, immunity, and metabolism [56].

The pathway enrichment analysis revealed that miR-96-5p plays a fundamental role in the formation and development of DR through multiple signaling pathways, including AGE-RAGE, insulin resistance, PI3K/AKT, mTOR, receptor tyrosine kinase, focal adhesion, and FOXO. The important genes were identified by centrality analysis, and the effect of miR-96-5p on their expression was determined by quantitative real-time PCR and Western blot assay.

Genes were determined based on the following factors: (i) high scores in all kinds of centralities, except bridging, clustering coefficient, neighborhood connectivity, and topological coefficient (AKT1, PIK3R1, and AKT2); high scores in all kinds of centralities, except bridging and topological coefficient (PIK3CA and AKT3); high scores in all kinds of centralities, except eccentricity, eigenvector, clustering coefficient, neighborhood connectivity, and topological coefficient (RAB2A and FOXO3); high scores in all kinds of centralities, except clustering coefficient, neighborhood connectivity, and topological coefficient (PRKCE); high scores in all kinds of centralities, except bridging and eccentricity (PRKCZ); high scores in all kinds of centralities, except bridging and betweenness centralities (IRS1); high scores in all kinds of centralities, except betweenness, eccentricity, eigenvector, clustering coefficient, and topological coefficient (SNAP23); and high scores in all kinds of centralities except betweenness, bridging, and eccentricity (FOXO1). In the next step, the following criteria were considered: high scores in clustering coefficient, neighborhood connectivity, and topological coefficient (SGK3); high scores in bridging, closeness centralities, radiality, and clustering coefficient (PDK2); high scores in bridging, centroid, and closeness centralities (EHD1); high scores in betweenness, centroid, closeness centralities, degree, and eigenvector (Pak1); and finally, high scores in bridging, centroid, closeness, degree, radiality, and stress (FOXO4).

According to our findings, miR-96-5p interferes not only with the expression of genes involved in the INS/AKT axis but also with the expression of genes implicated in GLUT4 translocation, which is associated with the dysregulation of cellular glucose utilization and metabolism [56]. In particular, the accumulation of extracellular glucose leads to the formation of AGEs, which triggers the inflammatory signaling pathways [1,57,58].

Activated AKT and serum/glucocorticoid inducible kinase (SGK) phosphorylate members of FOXO, which play important roles in cellular metabolism, inflammation, and survival. FOXO phosphorylation promotes the association with the 14-3-3 protein, resulting in its cytoplasmic retention, repression of target gene expression, and its degradation [59–62]. The results of qPCR and Western blot assay suggested that FOXOs were upregulated in miR-96-5p-overexpressing cells, but their expression was decreased at the protein level in the control group and miR-96-5p/antagomiR-96-treated cells. The activation of FOXOs regulates cell fate through apoptosis, cell cycle

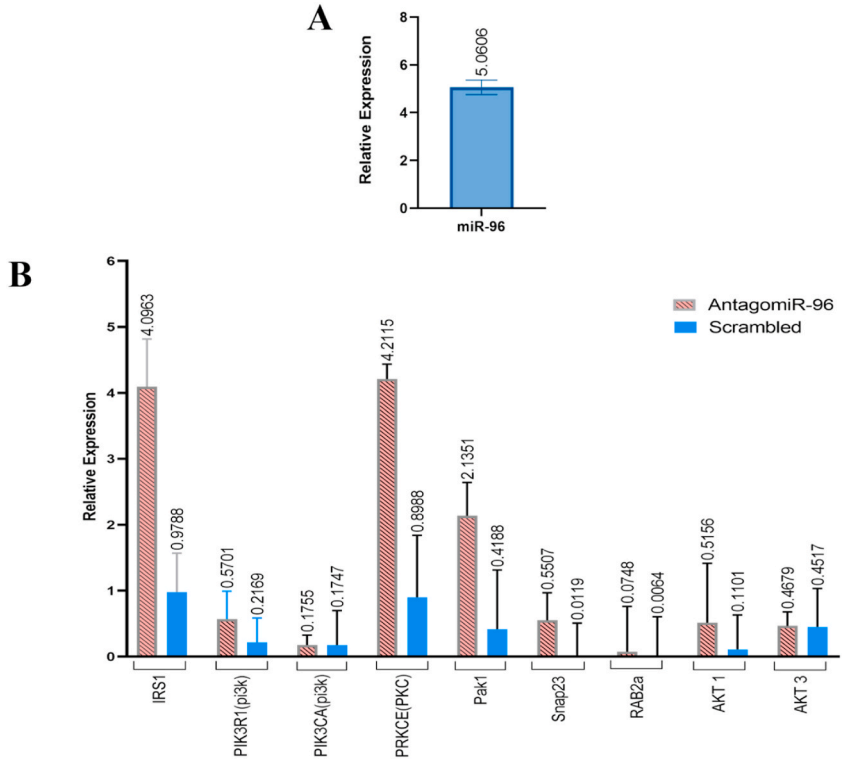

Fig. 8. **A.** gene expression analysis of miR-96 in mRPE cells cultured under HG conditions. Expression of miR-96 showed 5-fold increase under HG condition in comparison to the normal glucose level. **B.** Real-Time PCR analysis of miR-96-5p target genes in HG conditions with simultaneously antagomiR-96 or scrambled transfection. This data was calculated by dividing the relative expression under the 5 mM glucose treatment compared to the corresponding mannitol control and by dividing the relative expression under 30 mM glucose treatment compared to the corresponding mannitol control. Expression of desired genes were also shown in the plot. At least three independent experiments in triplicate were performed for each bar. GraphPad Prism 8 was used for drawing plots and one-way ANOVA test was used for data analysis. Error bars represent means ± SE, *P < 0.05.

progression, autophagy, oxidative stress resistance, and gluconeogenesis [63]. FOXO1 is upregulated in STZ-induced diabetic rats [64]. It was demonstrated that FOXO1 regulates the expression of VEGF and promotes angiogenesis [65]. In the present study, the relative expression levels of FOXO3 and FOXO4 were increased in human DR samples as compared to that in normal donors.

The growth and migration of hypopharyngeal carcinoma and pancreatic carcinoma cells can be inhibited in the presence of miR-96-5p. However, miR-96-5p promoted cell proliferation, migration, and invasion of breast cancer cells [66–70]. We observed that miR-96-5p overexpression reduced cell proliferation and increased cell migration of mRPE cells. Decreased cell proliferation might be due to miR-96-5p-induced upregulation of FOXO. According to previous studies, FOXO1 upregulation is associated with DR through increased apoptosis of microvascular endothelial cells and pericytes [59,71]. As mentioned earlier, TUNEL staining showed that TUNEL-positive cells were detected in the GCL, INL, and ONL layers of the retina in STZ-induced diabetic mice and AAV-2-eGFP-miR-96-treated mice. The migration of miR-96-5p-overexpressing mRPE cells and miR-96-5p/scrambled molecule--transfected cells was increased as compared to that of the control group, GFP-overexpressing cells, and miR-96-5p/antagomiR-96-treated cells. A previous study showed that FOXO activation promoted wound healing [59]. Enhanced cell migration in miR-96-5p-overexpressing cultures may be related to FOXO activation, which was confirmed in miR-96-5p/antagomiR-96-transfected and control groups. Real-time PCR and Western blot assay showed that FOXO1 expression was increased following miR-96-5p overexpression. This event might be due to the downregulation of SGK3 and AKTs, the antagonists of FOXO genes. Recently, miR-96-5p has been approved to promote migration and tube formation of human retinal microvascular endothelial cells [22]. Our findings revealed that mmu-miR-96-5p also significantly increased the tube formation rate of HUVEC cells as compared to that in the controls.

In the retinas of mice that received AAV-2-eGFP-miR-96 intravitreally and in diabetic mice, the vessel length was increased as compared to that in the control groups. This finding confirms the immediate role of miR-96-5p in angiogenesis. HE staining showed that INL, IRL, and whole retina thicknesses were decreased in STZ-induced diabetic mice as compared to that in the non-diabetic control and in AAV-2-eGFP-miR-96-injected mice as compared to that in AAV-2-eGFP-treated mice.

Real-time PCR results suggest that miR-96-5p interferes with the expression of some genes involved in the INS/AKT/GLUT4 signaling pathway, such as PIK3R1, PIK3CA, PRKCE, AKT1, AKT2, AKT3, SGK3, Pak1, Snap23, RAB2a, and Ehd1. According to miRNA target prediction databases such as TargetScan, these genes are the direct targets of miR-96-5p. Following treatment with antagomiR-

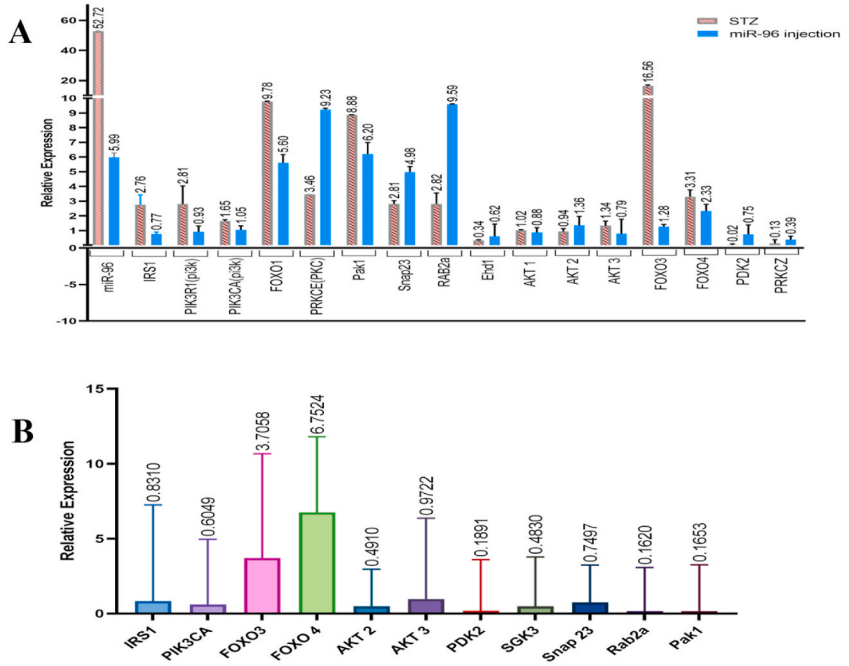

Fig. 9. Real-Time PCR of miR-96-5p and its target genes in mice and human retina. Data was obtained by the relative expression of the STZ induced diabetic mice compared to the control mice, and the mice injected intravitreally with AAV2-eGFP-miR-96 viruses compared to the AAV2-eGFP injected mice **(A)**. For plot **B**, data was obtained by relative expression of diabetic retinopathy retina donors in comparison to normal retina donors. The plot was drawn using GraphPad Prism 8. One-way ANOVA test was performed for data analysis. Error bars represent means ± SD ($n > 3$ *$P < 0.05$).

96, the expression levels of these genes were increased as compared to that in samples treated with scrambled control miRNA. Protein analysis also suggested that the expression levels of PIK3R1 and AKT1 were decreased and increased in the presence of miR-96-5p and antagomiR-96, respectively. The expression of PDK2 transcript increased after miR-96-5p overexpression. However, its expression was not detected following miR-96-5p/antagomiR-96 treatment. Western blot assay also revealed that the PDK2 protein was down-regulated in miR-96-5p-treated cells and miR-96-5p/scrambled-treated cells as compared to that in the control group, GFP-overexpressing cells, and miR-96-5p/antagomiR-96-treated groups. A previous study demonstrated that in high-fat diet mice, an insulin resistance model, miR-96-5p interferes with the insulin signaling pathway by directly targeting the 3'-UTRs of IRS1 and INSR mRNAs [56].

mRPE cultures when exposed to HG conditions mimic DR conditions and can be regarded as an in vitro model. These cultures exhibit fluctuation in the expression of numerous miRNAs and consequently several genes. miR-96-5p expression showed 5-fold increase under HG conditions as compared to that in normal glucose-treated cultures. Interestingly, the expression levels of genes involved in the INS/AKT/GLUT4 signaling pathway under HG conditions with simultaneous antagomiR-96 transfection were increased as compared to that following scrambled molecule transfection, including IRS1, PIK3R1, PIK3CA, PRKCE, AKT1, AKT3, Pak1, Snap23, and RAB2a.

Gene expression analysis by real-time PCR in STZ-induced diabetic mice retina revealed that the expression of miR-96-5p was increased by 52.72-fold as compared to that in the control group. This implies that miR-96-5p is effective in diabetic conditions. Moreover, the fold change of many of the selected genes was increased, including IRS1, PIK3R1, PIK3CA, FOXO1, PRKCE, Pak1, Snap23, RAB2a, AKT 3, FOXO3, and FOXO4. In contrast, the expression level of Ehd1, PDK2, AKT 2, and PRKCZ genes was decreased. AKT1 expression showed no significant changes. This might be due to a severe disturbance that occurs in the metabolism of diabetic animals. The gene expression pattern of AAV-2-eGFP-miR-96-treated mice indicated that the expression of miR-96-5p, FOXO1, PRKCE, Pak1, Snap23, RAB2a, AKT2, FOXO3, and FOXO4 was increased. However, the transcript levels of IRS1, PIK3R1, Ehd1, AKT1, AKT3, PDK2, and PRKCZ were decreased. In both diabetic and miR-96-5p-treated mice, the expression levels of miR-96-5p, FOXOs, PRKCE, Pak1, Snap23, and RAB2a were increased, while the mRNA transcript levels of Ehd1, PDK2, and PRKCZ were decreased. This indicates some similarities in the pattern of gene expression in STZ-induced diabetic mice and AAV-2-eGFP-miR-96-treated mice. Real-time PCR results for DR retina samples showed that the relative expression levels of IRS1, PIK3CA, AKT2, AKT3, PDK2, SGK3, Snap23, RAB2a, and Pak1 genes were decreased and the expression levels of FOXO3 and FOXO4 genes were increased as compared to those of their controls. These results suggest that miR-96-5p plays a role in the pathogenicity of DR by interfering with the INS/AKT/GLUT4 axis. This phenomenon, i.e., impairment of insulin signaling, is exactly the process that occurs during insulin resistance [57,72,73]. If miR-96 is inhibited in the early stages of the development of diabetic retinopathy, probably could prevent the progression of the disease. On the other hand, miRNAs have many effects on various biological pathways so, more studies are needed to achieve

comprehensive information about the effects of antagomiR-96 in physiological functions of the related organisms.

6. Conclusions

In conclusion, our findings identified that the miR-96-5p levels were significantly elevated in both mouse and cell models of DR. We found a novel molecular mechanism for effect of miR-96-5p on pathogenicity of DR. miR-96-5p downregulates the expression of several genes involved in INS/AKT/GLUT4 axis which can cause insulin resistance. Moreover, our results indicated that miR-96-5p could increase mobility, apoptosis and angiogenesis in the retina. Consequently, we suggest that inhibition of miR-96-5p may be a promising approach for controlling DR.

Declarations

Ethics approval and consent to participate

Ethical approval was waived by the local Ethics Committee of National Institute of Genetic Engineering and Biotechnology (NIGEB) in view of the retrospective nature of the study and all the procedures being performed were part of the routine care.

Consent for publication

All authors reviewed the results and contributed to the final manuscript and approved this manuscript for publication.

Author contribution statement

Narges Zolfaghari: Conceived and designed the experiments, Performed the experiments, Analyzed and interpreted the data; Wrote the paper.

Zahra-Soheila Soheili: Conceived and designed the experiments, Contributed reagents, materials, analysis tools or data; Wrote the paper.

Shahram Samiei: Performed the experiments.

Hamid Latifi-Navid: Performed the experiments, Analyzed and interpreted the data; Wrote the paper.

Ali Hafezi-Moghadam: Conceived and designed the experiments.

Hamid Ahmadieh: Conceived and designed the experiments; Wrote the paper.

Mozhgan Rezaei-Kanavi: Contributed reagents, materials, analysis tools or data.

Funding statement

Dr Zahra-Soheila Soheili was supported byNational Institute for Genetic Engineering and Biotechnology{727}.

Data availability statement

Data will be made availableon request.

Declaration of interest's statement

The authors confirm that there are no conflicts of interest.

Acknowledgements

We wish to acknowledge staff of Blood Transfusion Research Center and ophthalmic research center for contribution in this work.

Appendix A. Supplementary data

Supplementary data to this article can be found online at https://doi.org/10.1016/j.heliyon.2023.e15539.

References

[1] N. Butt, et al., Association of serum advanced glycation (AGEs) end products, apolipoprotein-B and zinc in severity of T2DM retinopathy, Pak. J. Pharm. Sci. 34 (2) (2021) 803–808.

[2] A. Das, P.G. McGuire, S. Rangasamy, Diabetic macular edema: pathophysiology and novel therapeutic targets, Ophthalmology 122 (7) (2015) 1375–1394.

[3] J. Quiroz, A. Yazdanyar, Animal models of diabetic retinopathy, Ann. Transl. Med. 9 (15) (2021).

[4] É. Csősz, et al., Diabetic retinopathy: proteomic approaches to help the differential diagnosis and to understand the underlying molecular mechanisms, J. Proteonomics 150 (2017) 351–358.
[5] X. Sun, et al., High glucose induces HSP47 expression and promotes the secretion of inflammatory factors through the IRE1α/XBP1/HIF-1α pathway in retinal Müller cells, Exp. Ther. Med. 22 (6) (2021) 1–8.
[6] M.F. Ercisli, et al., Diabetic retinopathy: mechanisms, and upcoming biomarkers, Centr. Asi. J. Med. Pharm. Sci. Innov. 1 (3) (2021) 131–142.
[7] K. Shao, et al., MicroRNA-139-5p Alleviates High Glucose-Triggered Human Retinal Pigment Epithelial Cell Injury by Targeting LIM-Only Factor 4, Mediators of Inflammation, 2021, p. 2021.
[8] M. Ponnalagu, et al., Retinal pigment epithelium-secretome: a diabetic retinopathy perspective, Cytokine 95 (2017) 126–135.
[9] W. Du, et al., Protection of kaempferol on oxidative stress-induced retinal pigment epithelial cell damage, Oxid. Med. Cell. Longev. 2018 (2018).
[10] J.R. Jaldin-Fincati, et al., Update on GLUT4 vesicle traffic: a cornerstone of insulin action, Trends Endocrinol. Metabol. 28 (8) (2017) 597–611.
[11] Y. Sharma, et al., Advanced glycation end products and diabetic retinopathy, J. Ocul. Biol. Dis. Infor. 5 (3–4) (2012) 63–69.
[12] P. Fasanaro, et al., microRNA: emerging therapeutic targets in acute ischemic diseases, Pharmacol. Ther. 125 (1) (2010) 92–104.
[13] R. Natarajan, S. Putta, M. Kato, MicroRNAs and diabetic complications, J. Cardiovas. Trans. Res. 5 (4) (2012) 413–422.
[14] K. McArthur, et al., MicroRNA-200b regulates vascular endothelial growth factor–mediated alterations in diabetic retinopathy, Diabetes 60 (4) (2011) 1314–1323.
[15] Q. Gong, G. Su, Roles of miRNAs and long noncoding RNAs in the progression of diabetic retinopathy, Biosci. Rep. 37 (6) (2017).
[16] Q. Gong, et al., Differentially expressed microRNAs in the development of early diabetic retinopathy, J. Diabetes Res. 2017 (2017).
[17] Z. Smit-McBride, L.S. Morse, MicroRNA and diabetic retinopathy—biomarkers and novel therapeutics, Ann. Transl. Med. 9 (15) (2021).
[18] S. Xu, microRNA expression in the eyes and their significance in relation to functions, Prog. Retin. Eye Res. 28 (2) (2009) 87–116.
[19] Q. Zhu, et al., Sponge transgenic mouse model reveals important roles for the microRNA-183 (miR-183)/96/182 cluster in postmitotic photoreceptors of the retina, J. Biol. Chem. 286 (36) (2011) 31749–31760.
[20] Y. Ma, et al., Dysregulation and functional roles of miR-183-96-182 cluster in cancer cell proliferation, invasion and metastasis, Oncotarget 7 (27) (2016), 42805.
[21] M. Desjarlais, et al., MicroRNA expression profile in retina and choroid in oxygen-induced retinopathy model, PLoS One 14 (6) (2019) e0218282.
[22] M. Desjarlais, et al., MicroRNA-96 promotes vascular repair in oxygen-induced retinopathy—a novel uncovered vasoprotective function, Front. Pharmacol. 11 (2020) 13.
[23] J.A. Santiago, J.A. Potashkin, A network approach to clinical intervention in neurodegenerative diseases, Trends Mol. Med. 20 (12) (2014) 694–703.
[24] J. Pinero, et al., DisGeNET: a Discovery Platform for the Dynamical Exploration of Human Diseases and Their Genes, Database, Oxford), 2015, p. bav028, 2015.
[25] J. Pinero, et al., The DisGeNET knowledge platform for disease genomics: 2019 update, Nucleic Acids Res. 48 (D1) (2020) D845–D855.
[26] D. Szklarczyk, et al., The STRING database in 2021: customizable protein-protein networks, and functional characterization of user-uploaded gene/measurement sets, Nucleic Acids Res. 49 (D1) (2021) D605–D612.
[27] D. Szklarczyk, et al., STRING v11: protein-protein association networks with increased coverage, supporting functional discovery in genome-wide experimental datasets, Nucleic Acids Res. 47 (D1) (2019) D607–D613.
[28] T. Sheils, et al., How to illuminate the druggable genome using pharos, Curr. Prot. Bioinform> 69 (1) (2020) e92.
[29] V. Agarwal, et al., Predicting effective microRNA target sites in mammalian mRNAs, Elife 4 (2015).
[30] M. Kanehisa, S. Goto, KEGG: kyoto encyclopedia of genes and genomes, Nucleic Acids Res. 28 (1) (2000) 27–30.
[31] D. Warde-Farley, et al., The GeneMANIA prediction server: biological network integration for gene prioritization and predicting gene function, Nucleic Acids Res. 38 (2010) W214–W220 (Web Server issue).
[32] P. Shannon, et al., Cytoscape: a software environment for integrated models of biomolecular interaction networks, Genome Res. 13 (11) (2003) 2498–2504.
[33] G.D. Bader, C.W. Hogue, An automated method for finding molecular complexes in large protein interaction networks, BMC Bioinf. 4 (2003) 2.
[34] G. Scardoni, et al., Biological network analysis with CentiScaPe: centralities and experimental dataset integration, F1000Res 3 (2014) 139.
[35] G. Scardoni, M. Petterlini, C. Laudanna, Analyzing biological network parameters with CentiScaPe, Bioinformatics 25 (21) (2009) 2857–2859.
[36] Y. Assenov, et al., Computing topological parameters of biological networks, Bioinformatics 24 (2) (2008) 282–284.
[37] D.W. Huang, et al., DAVID Bioinformatics Resources: expanded annotation database and novel algorithms to better extract biology from large gene lists, Nucleic Acids Res. 35 (2007) W169–W175 (Web Server issue).
[38] U. Raudvere, et al., g:Profiler: a web server for functional enrichment analysis and conversions of gene lists (2019 update), Nucleic Acids Res. 47 (W1) (2019) W191–W198.
[39] A. Fabregat, et al., The reactome pathway knowledgebase, Nucleic Acids Res. 46 (D1) (2018) D649–D655.
[40] F. Supek, et al., REVIGO summarizes and visualizes long lists of gene ontology terms, PLoS One 6 (7) (2011), e21800.
[41] T. Mishima, et al., Determinants of effective lentivirus-driven microRNA expression in vivo, Sci. Rep. 6 (1) (2016), 33345.
[42] M. Davari, et al., Overexpression of miR-183/-96/-182 triggers neuronal cell fate in Human Retinal Pigment Epithelial (hRPE) cells in culture, Biochem. Biophys. Res. Commun. 483 (1) (2017) 745–751.
[43] E.R. Pirmardan, et al., Characterization of a spontaneously generated murine retinal pigmented epithelium cell line; a model for in vitro experiments, Exp. Cell Res. 347 (2) (2016) 332–338.
[44] E.R. Pirmardan, et al., Vivo evaluation of PAX6 overexpression and NMDA cytotoxicity to stimulate proliferation in the mouse retina, Sci. Rep. 8 (1) (2018) 1–10.
[45] B. Dalby, et al., Advanced transfection with Lipofectamine 2000 reagent: primary neurons, siRNA, and high-throughput applications, Methods 33 (2) (2004) 95–103.
[46] H.S. Najafabadi, et al., Optogenetic control of neural differentiation in Opto-mGluR6 engineered retinal pigment epithelial cell line and mesenchymal stem cells, J. Cell. Biochem. (2021).
[47] S. Taghizadeh, et al., sFLT01 modulates invasion and metastasis in prostate cancer DU145 cells by inhibition of VEGF/GRP78/MMP2&9 axis, BMC Mol. Cell Biol. 22 (1) (2021) 1–11.
[48] C. McClure, et al., Production and titering of recombinant adeno-associated viral vectors, J. Vis. Exp. (57) (2011).
[49] Manual, I., AAV Helper-free System.
[50] B.L. Furman, Streptozotocin-induced diabetic models in mice and rats, Curr. Protoc. Pharmacol. 70 (1) (2015) 5.47. 1–5.47. 20.
[51] T.M. Lehti, et al., Effects of streptozotocin-induced diabetes and physical training on gene expression of extracellular matrix proteins in mouse skeletal muscle, Am. J. Physiol. Endocrinol. Metab. 290 (5) (2006) E900–E907.
[52] A.H. Fischer, et al., Hematoxylin and eosin staining of tissue and cell sections, Cold Spring Harb. Protoc. 2008 (5) (2008) prot4986.
[53] M.F. Kramer, Stem-loop RT-qPCR for miRNAs, 10. 1-15.10. 15, Curr. Protoc. Mol. Biol. 95 (1) (2011) 15.
[54] S. Dambal, et al., The microRNA-183 cluster: the family that plays together stays together, Nucleic Acids Res. 43 (15) (2015) 7173–7188.
[55] M. Tanaka, et al., EVI1 oncogene promotes KRAS pathway through suppression of microRNA-96 in pancreatic carcinogenesis, Oncogene 33 (19) (2014) 2454–2463.
[56] W.-M. Yang, K.-H. Min, W. Lee, Induction of miR-96 by dietary saturated fatty acids exacerbates hepatic insulin resistance through the suppression of INSR and IRS-1, PLoS One 11 (12) (2016) e0169039.
[57] P.-T. Xu, et al., Impaired translocation of GLUT4 results in insulin resistance of atrophic soleus muscle, BioMed Res. Int. 2015 (2015).
[58] G. Ramm, et al., A role for 14-3-3 in insulin-stimulated GLUT4 translocation through its interaction with the RabGAP AS160, J. Biol. Chem. 281 (39) (2006) 29174–29180.
[59] Y. Wang, Y. Zhou, D.T. Graves, FOXO transcription factors: their clinical significance and regulation, BioMed Res. Int. 2014 (2014).
[60] N. Kodani, J. Nakae, Tissue-specific metabolic regulation of FOXO-binding protein: FOXO does not act alone, Cells 9 (3) (2020) 702.

[61] D.R. Plas, C.B. Thompson, Akt activation promotes degradation of tuberin and FOXO3a via the proteasome, J. Biol. Chem. 278 (14) (2003) 12361–12366.
[62] H. Matsuzaki, et al., Insulin-induced phosphorylation of FKHR (Foxo1) targets to proteasomal degradation, Proc. Natl. Acad. Sci. USA 100 (20) (2003) 11285–11290.
[63] M.E. Carter, A. Brunet, FOXO transcription factors, Curr. Biol. 17 (4) (2007) R113–R114.
[64] J. Liu, et al., Up-regulation of FoxO1 contributes to adverse vascular remodelling in type 1 diabetic rats, J. Cell Mol. Med. 24 (23) (2020) 13727–13738.
[65] H.H. Jeon, et al., FOXO1 regulates VEGFA expression and promotes angiogenesis in healing wounds, J. Pathol. 245 (3) (2018) 258–264.
[66] W. Liao, et al., Up-regulation of miR-96-5p inhibits the proliferation of FaDu cell line by targeting mTOR, Nanosci. Nanotechnol. Lett. 9 (12) (2017) 2013–2021.
[67] C. Li, et al., GPC1 regulated by miR-96-5p, rather than miR-182-5p, in inhibition of pancreatic carcinoma cell proliferation, Int. J. Mol. Sci. 15 (4) (2014) 6314–6327.
[68] Y. Hong, et al., miR-96 promotes cell proliferation, migration and invasion by targeting PTPN9 in breast cancer, Sci. Rep. 6 (1) (2016) 1–16.
[69] W.y. Qin, et al., MiR-96-5p promotes breast cancer migration by activating MEK/ERK signaling, J. Gene Med. 22 (8) (2020) e3188.
[70] H. Lin, et al., Unregulated miR-96 induces cell proliferation in human breast cancer by downregulating transcriptional factor FOXO3a, PLoS One 5 (12) (2010), e15797.
[71] Y. Behl, et al., FOXO1 plays an important role in enhanced microvascular cell apoptosis and microvascular cell loss in type 1 and type 2 diabetic rats, Diabetes 58 (4) (2009) 917–925.
[72] Y. Xing, et al., Reduction of the PI3K/Akt related signaling activities in skeletal muscle tissues involves insulin resistance in intrauterine growth restriction rats with catch-up growth, PLoS One 14 (5) (2019) e0216665.
[73] X. Huang, et al., The PI3K/AKT pathway in obesity and type 2 diabetes, Int. J. Biol. Sci. 14 (11) (2018) 1483.
[74] Z. Ji, et al., miR-7a targets insulin receptor substrate-2 gene and suppresses viability and invasion of cells in diabetic retinopathy mice via PI3K-Akt-VEGF pathway, Diabetes, Metab. Syndrome Obes. Targets Ther. 14 (2021) 719.
[75] W.M. Valencia, H. Florez, How to prevent the microvascular complications of type 2 diabetes beyond glucose control, BMJ (2017) 356.
[76] Y.-N. Du, et al., SGK1-FoxO1 signaling pathway mediates Th17/Treg imbalance and target organ inflammation in angiotensin II-induced hypertension, Front. Physiol. 9 (2018) 1581.
[77] V.A. Lizunov, et al., Insulin stimulates the halting, tethering, and fusion of mobile GLUT4 vesicles in rat adipose cells, J. Cell Biol. 169 (3) (2005) 481–489.
[78] K. Sakamoto, G.D. Holman, Emerging role for AS160/TBC1D4 and TBC1D1 in the regulation of GLUT4 traffic, Am. J. Phys. Endocrin. Metab. 295 (1) (2008) E29–E37.
[79] S.-X. Tan, et al., The Rab GTPase-activating protein TBC1D4/AS160 contains an atypical phosphotyrosine-binding domain that interacts with plasma membrane phospholipids to facilitate GLUT4 trafficking in adipocytes, Mol. Cell Biol. 32 (24) (2012) 4946–4959.
[80] K. Fecchi, et al., Spatial and temporal regulation of GLUT4 translocation by flotillin-1 and caveolin-3 in skeletal muscle cells, Faseb. J. 20 (6) (2006) 705–707.
[81] C.B. Chiribau, et al., FOXO3A regulates peroxiredoxin III expression in human cardiac fibroblasts, J. Biol. Chem. 283 (13) (2008) 8211–8217.
[82] M. Farhan, et al., FOXO signaling pathways as therapeutic targets in cancer, Int. J. Biol. Sci. 13 (7) (2017) 815.
[83] L. Sylow, et al., Rac1 signaling is required for insulin-stimulated glucose uptake and is dysregulated in insulin-resistant murine and human skeletal muscle, Diabetes 62 (6) (2013) 1865–1875.
[84] T. Kawaguchi, et al., The t-SNAREs syntaxin4 and SNAP23 but not v-SNARE VAMP2 are indispensable to tether GLUT4 vesicles at the plasma membrane in adipocyte, Biochem. Biophys. Res. Commun. 391 (3) (2010) 1336–1341.